

Study of the Berezinskii-Kosterlitz-Thouless transition: An unsupervised machine learning approach

Sumit Haldar,¹ Sk Saniur Rahaman,¹ and Manoranjan Kumar^{1,*}

¹*S. N. Bose National Centre for Basic Sciences,
J D Block, Sector III, Salt Lake City, Kolkata 700106*

The Berezinskii-Kosterlitz-Thouless (BKT) transition in magnetic system is an intriguing phenomena and an accurate estimation of the BKT transition temperature has been a long-standing problem. In this work we explore the anisotropic classical Heisenberg XY and XXZ models with ferromagnetic exchange on a square lattice and antiferromagnetic exchange on a triangular lattice using an unsupervised machine learning approach called principal component analysis (PCA). In earlier studies of the BKT transition, spin configurations and vorticities calculated from Monte Carlo method are used to determine the transition temperature T_{BKT} , but those methods fail to give any conclusive results by analyzing the principal components in the PCA approach. In this work vorticities are used as initial input to the PCA and curve of the first principal component with temperature is fitted with a function to determine an accurate value of T_{BKT} . This procedure works well for anisotropic classical Heisenberg with ferromagnetic exchange on square lattice as well as for frustrated antiferromagnetic exchange on a triangular lattice. The classical anisotropic Heisenberg antiferromagnetic model on the triangular lattice has two close transitions; the BKT at T_{BKT} and Ising like phase transition for chirality at T_c and it is difficult to separate these transition points. It is also noted that using the PCA method and manipulation of their first principal component, not only separation of transition points are possible but also transition temperature can be determined accurately.

I. INTRODUCTION

In the last decade, information or data has become an indispensable resource and is transforming our daily life very rapidly. Unfortunately, extracting the relevant data out of monumental volume of the information is one of the biggest challenges. Machine learning (ML) is an efficient and elegant tool to get relevant information out of large data. Machine learning algorithms can be divided into two broad categories (i) supervised and (ii) unsupervised depending upon training the dataset. In the supervised algorithm, machine trained with labeled data set and identifies the unlabelled data with high accuracy, whereas, an unsupervised algorithm does not depend on the labeled data set, it automatically detects the structure from a noisy data set [1–3].

In the last few years availability of advanced computational facilities has made machine learning techniques a popular tool to analyze the problems of different academic and social domains. The ML based techniques have been rampantly used in our daily life such as in image recognition [4–7], advertising [8], social networking [9–11], engineering [12] and designing medicine [13] etc. In physical sciences like astrophysics [14], high energy physics [15], and biological physics [16, 17], the ML has extensive application, especially, in condensed matter this method is used to identify phase transitions [18–26]. Application of the ML is still in a nascent stage in the condensed matter and reproducing the well known results is still a primary goal. The unsupervised machine

learning techniques such as principal component analysis (PCA) [27, 28] has been successfully applied in combination with Monte Carlo (MC) to identify the thermal phase transition in classical frustrated [23, 26] and unfrustrated [22, 29, 30] model systems. On the other hand supervised machine learning such as convolutional and fully connected neural networks have been used successfully to classify symmetry-broken phases in many-body systems [19, 31–34].

The two dimensional classical anisotropic Heisenberg model does not have long range magnetic order at any finite temperature as rigorously stated by the Mermin-Wagner theorem [35]. However, the renormalization group [36] and free energy [37] calculations show that anisotropic Heisenberg model undergoes a phase transition for any deviation from the isotropic exchange limit at finite temperature T . The critical temperature goes as $1/\ln(1 - \Delta)$ where Δ is axial anisotropy in the system [38]. The phase transition in two dimensional XXZ model occurs due to vortex unbinding, and if the spin in vortices core pointing preferably out of plane direction then the model may display Berezinskii-Kosterlitz-Thouless(BKT) transition [39–41]. In process of phase transition the correlation function goes from quasi-long range order to short-range order on increasing T and the peak of specific heat is at higher than the T_{BKT} . The classical antiferromagnetic anisotropic Heisenberg model on a triangular lattice is a frustrated system, and in the XY model this system has two phases and their corresponding order parameters; in plane magnetization with continuous $SO(2)$ rotational symmetry and chirality with discrete Z_2 lattice reflection symmetry. The rotational group symmetry follows the Mermin-Wagner theorem and has short range order at finite temperature whereas

* manoranjan.kumar@bose.res.in

the discrete symmetries give rise to long range order and Ising like phase transition for chirality is allowed at finite temperature. Therefore, there are two transitions; the BKT transition at T_{BKT} and the chiral phase transition at T_c , however the difference between the two critical temperatures are small and their determination is still a challenge [42, 43]. Therefore, the application of the ML approach is a desirable to understand the two distinct phase transition points.

The ML approach is successful in predicting the order to disorder transition and it motivated scientists to explore the possibility of determination of the BKT phase transition [22, 26]. Beach *et al.* [44] used a neural network to study the BKT transition on a two-dimensional XY model and showed that feed forward networking was unable to identify the BKT transition point using the raw spin configurations obtained from MC simulations, but convolutional networking could predict the BKT point. They also showed that feeding vorticity calculated from the MC configurations in both the algorithms helps to predict T_{BKT} [44]. Hu *et al.* [26] pointed out the limitation of PCA to identify the BKT transition point in XY model on a two-dimensional square lattice. Furthermore, they also observed an exponential increase in the first principal component as a function of temperature near the BKT point by feeding absolute vorticity. Wang *et al.* have used temperature resolved PCA to study the phase transition points in XY model on an antiferromagnetic triangular lattice, although fails to separate both the temperature [23].

In the present study, we use the ML approach to study the BKT transition and absolute value of vorticity is used as input of PCA. In this method vorticities are calculated from spin configurations obtained from MC approach as in ref. [26]. We note that the first principal component p_1 exactly matches with density of vortex calculated from MC simulations. In this work, we also show that least-square fitting of p_1 with the function $a_0(1 - \frac{T_{BKT}}{T})^\alpha$ near the proliferation region can predict T_{BKT} close to the reported values [42, 45, 46]. T_{BKT} of XXZ model on square lattice is calculated as a function of Δ (anisotropy in the z -direction) using the PCA and compared with reported value in the literature [38]. In the second part we study the XY model on a triangular lattice and distinguish T_{BKT} due to vortex binding-unbinding and chirality phase transition T_c associated with discrete Z_2 symmetry. The XXZ model on the triangular lattice is also studied to calculate T_{BKT} and T_c using PCA and compared with reported results [43]. In this paper we show that chiral order parameter can be calculated using the PCA if we feed z -component of the chiral vector for XY and XXZ model systems.

The paper is organized as follows: we discuss the model Hamiltonians in section II. The principal component analysis is discussed in section III. Phase transition temperatures are calculated in section IV and it is divided into four subsections. In section V we conclude the paper with a summary.

II. MODEL HAMILTONIAN

We consider two anisotropic Heisenberg model: XY and XXZ model. The XXZ model is an anisotropic Heisenberg model having extra degree of freedom in z direction compared to XY model. The XY model Hamiltonian can be written as

$$H_{XY} = J \sum_{\langle ij \rangle} (S_i^x S_j^x + S_i^y S_j^y), \quad (1)$$

where J is the strength of the exchange interaction between nearest neighbour spins and S^x and S^y are x and y components of spins.

The anisotropic Heisenberg XXZ model can be written as

$$H_{XXZ} = J \sum_{\langle ij \rangle} (S_i^x S_j^x + S_i^y S_j^y + \Delta S_i^z S_j^z), \quad (2)$$

where (S^x, S^y, S^z) are the spin components along the x , y and z axes respectively. J can be set to -1 or 1 for ferromagnetic or antiferromagnetic systems. Δ accounts for the anisotropy in the z -direction and for $\Delta = 0$ Eq. 2 reduce to $XX0$ model. The $XX0$ model has also spin fluctuation in the z direction as well and for $\Delta = 1$ this model called isotropic Heisenberg model.

III. PRINCIPAL COMPONENT ANALYSIS

The PCA is an orthogonal linear transformation procedure to reduce the dimension of multi-dimensionality of the data set without losing the information in the data. In the new rotated basis most of the variations are confined to only a few dimensions and other dimensions are irrelevant. First we construct a data matrix Y using the snapshot of spin configurations at different sites calculated from conventional Metropolis Monte Carlo (MC) simulations and it has L dimensional features and $N_T = M \times m$ dimensional of samples. In this case M evenly separated temperatures are considered with m number of spin configurations at every T . The data-centred matrix X is calculating as $X_{i,k} = Y_{i,k} - \mu_i$, where, μ_i is defined as $\mu_i = \frac{1}{N_T} \sum_{k=1}^{N_T} Y_{i,k}$ [26]. The covariance matrix can be defined as

$$C_T(i, j) = \sum_{k=1}^{N_T} X_{i,k} X_{j,k}^T. \quad (3)$$

where $X_{k,j}^T$ is the transpose of $X_{j,k}$. The dimension of C_T is $L \times L$. Diagonalization of C_T gives L eigenvalues $[\lambda_1, \dots, \lambda_L]$ and corresponding eigenvectors $[w_1, \dots, w_L]$. One can also write,

$$X X^T w_l = \lambda_l w_l \quad (4)$$

where, each eigenvector is a column vector with L rows. The variance of the data set for various T decreases from the largest to smallest eigenvalues, therefore, due to dimensionality reduction procedure, we find that only few eigenvectors corresponding to the largest eigenvalues are important to give accurate description of original data. The number of principal components N_T is obtained by projecting the original data along l^{th} eigenvector w_l and the l^{th} principal component $p_l(T, k)$ corresponding to the k^{th} sample can be defined as

$$p_l(T, k) = w_l^T Y(k) \quad (5)$$

where, $Y(k)$ is the k^{th} sample with L entries of the data matrix Y , and w_l^T is the transpose of the eigenvector w_l . The l^{th} ‘quantified principal component’ is defined by adding up the principal components over the samples (m) for a particular T value.

$$p_l(T) = \sum_{k=1}^m |p_l(T, k)| \quad (6)$$

A. Input to the PCA

The PCA is sensitive to the initial input used for calculation and may fail to give any reasonable value of BKT transition temperature even if the absolute vorticities are used as initial input as shown by various groups [22, 23, 26]. The information of local vortex and antivortex structures are calculated from the snapshots of MC simulations. The vorticity is calculated using a contour integration

$$v = \oint_c \delta\theta dl = 2\pi k, \quad \text{where } k = \pm 1, \pm 2, \dots \quad (7)$$

where c refers to contour around each plaquette of the square lattice, and $k = +1, -1$ corresponds to vortex and anti-vortex structures respectively. $\delta\theta [-2\pi, 2\pi]$ is angle difference between nearest-neighbor spins of each plaquette, converts it to the range $[-\pi, \pi]$ using a saw-tooth function

$$Saw(\theta) = \begin{cases} \theta + 2\pi, & \theta \leq -\pi, \\ \theta, & -\pi \leq \theta \leq \pi, \\ \theta - 2\pi, & \pi \leq \theta \end{cases}$$

A schematic representation of local vortex and anti-vortex structure is shown in Fig. 1. The absolute value of vorticities are used to construct the data matrix Y and data centered matrix X . Covariance matrix C_T is constructed using X and the first principal component p_1 corresponding to the largest eigenvalue of C_T is constructed by taking the projection of Y along the largest eigenvector. Now ‘first quantified principal component’ p_1 as Eq. 6 is plotted as function of T and this function is similar to the vortex density and fitting this curve with a function $a_0(1 - \frac{T_{BKT}}{T})^\alpha$ we get T_{BKT} . We compare the

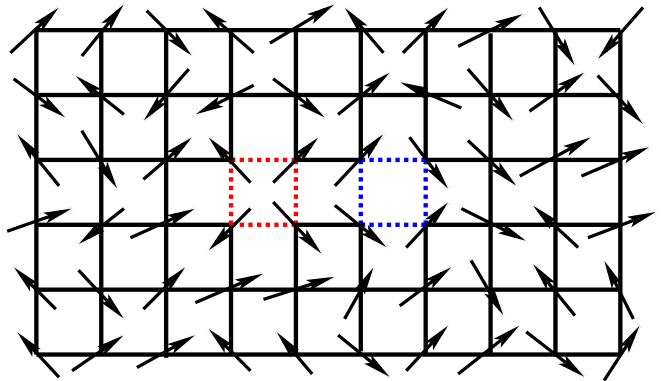


FIG. 1. Schematic representation of vortex and anti vortex configurations. The red contour is showing the vortex structure and the blue contour is showing the antivortex structure.

behaviour of p_1 with vortex densities which is defined as

$$\rho_v(T) = \frac{1}{(m * L^2)} \sum_{ij=1} v_{ij}(T) \quad (8)$$

where m is number of MC steps over which the snapshot of spin configurations are taken and $v_{ij}(T)$ is vorticity of the system of size L at T .

In order to determine chiral phase transition in triangular lattice, chirality vector is calculated using the raw spin configurations from MC simulations and the z-component of chirality is fed as a initial input to the PCA. The chirality vector between spins S_1, S_2 , and S_3 at the vertices of each elementary triangle can be defined as

$$\vec{\kappa}_i = \frac{2}{3\sqrt{3}} (\vec{S}_1 \times \vec{S}_2 + \vec{S}_2 \times \vec{S}_3 + \vec{S}_3 \times \vec{S}_1), \quad (9)$$

where the normalized factor comes because of the $2\pi/3$ structure. We have taken a consistent convention for each elementary triangle (anticlockwise for both upward and downward triangles). A schematic representation of 120° structures with our convention has been shown in Fig. 2. In the case of the XY model, spin can rotate only in the plane, so only κ^z component will contribute, whereas for XXZ model may have true chiral order. The scalar chirality gives us a sense of the rigidity of the 120° structure and to quantify the parameter, we define a quantity called staggered chirality as

$$\kappa = \frac{1}{N_T} \sum_i (-1)^i \kappa_i^z, \quad (10)$$

where $(-1)^i$ have positive and negative values for downward and upward triangles.

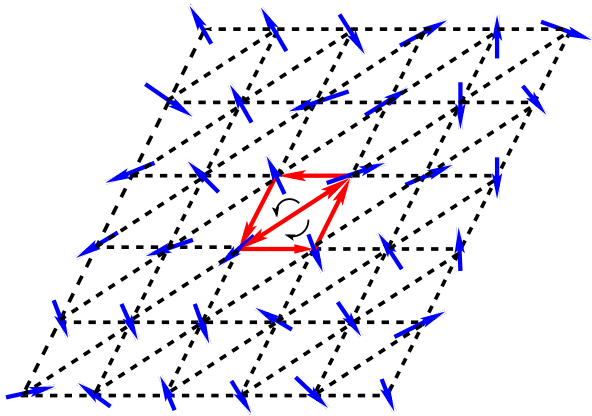


FIG. 2. Schematic representation of two types of chirality corresponding to the anticlockwise and clockwise rotation of the three spins at the vertices of the triangle.

IV. RESULTS AND DISCUSSION

In this section we first study the two dimensional ferromagnetic Heisenberg XY model on a square lattice and revisit the results of XY model on square lattice using the PCA method [26]. The vortex density ρ_v and the first principal component p_1 behaviours are compared as a function of temperature T . To extract T_{BKT} from p_1 , a standard function is used and to our surprise the extracted T_{BKT} matches quite well with reported values in the literature [42, 45, 46]. We also analyze the ferromagnetic XXZ model on a square lattice and find T_{BKT} using the PCA and compare with the reported results of the MC method [38]. We also use this approach to calculate T_{BKT} for antiferromagnetic XY and XXZ model on a triangular lattice. In this lattice systems T_c and T_{BKT} are quite close and their determination is a difficult task, we show that using PCA these two transitions can be easily recognised [43].

A. XY model on square lattice

In this subsection we study the BKT transition of classical Heisenberg model in Eq. 1 with ferromagnetic interaction on square lattice. The PCA approach is applied to study this model as explained in section III to extract an accurate T_{BKT} . The density of vortex ρ_v calculated using Eq. 8 is shown in Fig. 3 for three different system sizes $L = 30, 50$, and 100 which overlap with p_1 . All eigenvalues of C_T for ferromagnetic XY model on square lattice are plotted in the inset of Fig. 3(a). The largest eigenvalue λ_1 of $L = 100$ system is 180 times higher compared to other λ_k which are close to zero.

In Fig. 3(b), $p_1(T)$ as a function of T are shown for $L = 30, 50$, and 100 . p_1 increases gradually and its proliferation starts around $T/J \simeq 0.6$. However, in the literature the value of $T_{BKT} \approx 0.894$ in the thermodynamic limit, but proliferation of p_1 starts below $T < 0.65$.

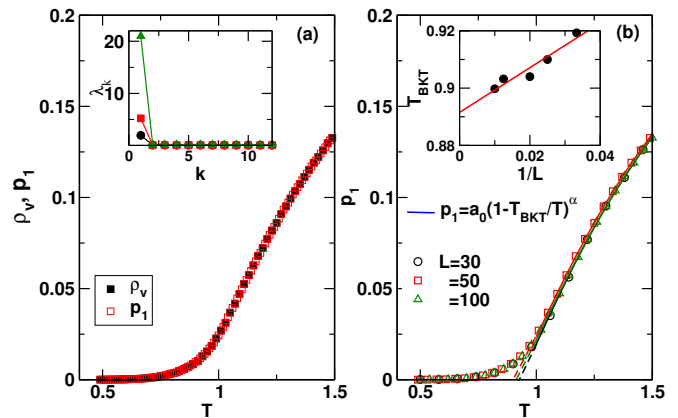


FIG. 3. (a) The vortex density ρ_v and p_1 as a function of temperature for XY model on a square lattice for $L = 50$. We consider $M = 51$ evenly separated temperature points from 0.5 to 1.5 with steps $\Delta T = 0.02$. At each temperature point we consider $m = 1000$ uncorrelated data samples. In the inset, eigenvalues are shown for $L = 30, 50$, and 100 . (b) p_1 as function of temperature T is fitted with the function $a_0(1 - \frac{T_{BKT}}{T})^\alpha$, where a_0, α are the fitting parameters. In the inset the finite size scaling is shown.

We fit the high T region with function $a_0(1 - \frac{T_{BKT}}{T})^\alpha$ and extracted T_{BKT} is 0.908, whereas the reported value is 0.894 and the fitting of $p_1(T)$ gives the same value of T_{BKT} . The finite size scaling of p_1 is shown in Fig. 3(b) and the extrapolated value of T_{BKT} is shown in the inset of Fig. 3(b). The extrapolated value is $T_{BKT} = 0.894$, which is consistent with the literature [42, 45, 46].

B. XXZ model on square lattice

Next, we investigate the thermal phase transition of XXZ model on a 2D square lattice using PCA and C_T is constructed using x, y , and z components of spins for $\Delta = 0.0, 0.25, 0.50, 0.75$, and 0.95 . To distinguish the BKT phase transition, we feed absolute value of the vorticity into PCA. In inset of Fig. 4(a) λ_k are shown and λ_1 is only dominant eigenvalue of C_T . Therefore, only p_1 is considered as shown in Fig. 4(a). p_1 curve for $\Delta = 0.0, 0.25, 0.5, 0.95$, and 0.99 are fitted with the function $a_0(1 - \frac{T_{BKT}}{T})^\alpha$, where a_0, T_{BKT} , and α are fitting parameters. In this case also p_1 exactly matches with vortex density in the system. The scatter plot of p_1 and p_2 is shown in Fig. 4(b) with temperature scale represented in color-bar. Table I shows the comparison of T_{BKT} with its value in the literature [38]. We notice that T_{BKT} is in good agreement with the reported value calculated from the MC method.

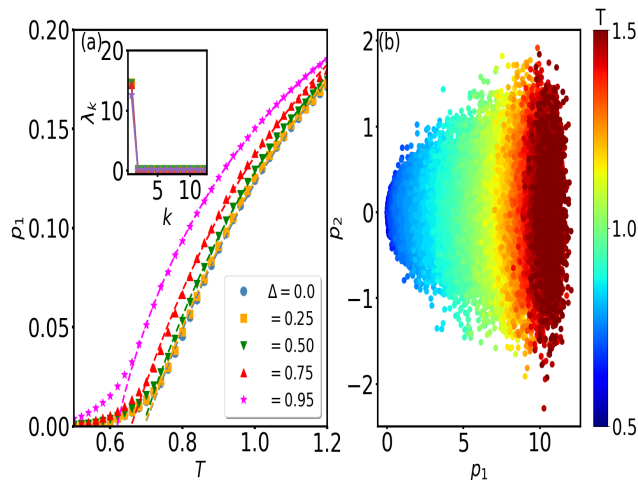


FIG. 4. PCA results of XXZ model on a square lattice by feeding the absolute vorticity for $\Delta = 0.0, 0.25, 0.5, 0.75,$ and 0.95 . (a) p_1 is fitted with the function $a_0(1 - \frac{T}{T_{BKT}})^\alpha$ for different Δ , and the eigenvalues are shown in the inset. (b) projection of absolute vorticity configurations along the axis with highest variance ratio, p_1 and the second highest, p_2 . The color-bar represents the temperature points in the range $T = 0.5$ to $T = 1.5$, with steps $\Delta = 0.02$.

TABLE I. BKT transition temperature T_{BKT} associated with unbinding of vortex-anti-vortex pair. Comparison between estimated results after fitting with function $a_0(1 - \frac{T}{T_{BKT}})^\alpha$ and the reported results using MC method. \pm values show the error bar of the fitting.

Δ	T_{BKT} (MC)	T_{BKT} (PCA)
0.00	0.699 ± 0.003	0.693 ± 0.002
0.25		0.692 ± 0.0002
0.50	0.687 ± 0.003	0.690 ± 0.002
0.75		0.657 ± 0.001
0.95	0.608 ± 0.004	0.614 ± 0.004

C. XY model on Triangular lattice

We focus on the antiferromagnetic classical Heisenberg model on a two-dimensional triangular lattice, the competing nearest neighbor antiferromagnetic interactions set a geometrical frustration in this system. In the case of the XY model, the frustration causes a collinear arrangement of spins with 120° angle between each other in each of the three sublattices [47, 48] and such ground-state can be two-fold degenerate as it is associated with discrete Z_2 lattice reflection. This system has two type of phase transition first BKT type which is associated with $SO(2)$ rotation symmetry and chirality transition which is associated with Z_2 reflection symmetry. In this model the BKT transition temperature T_{BKT} and chirality transition temperature T_c are close at 0.504 and 0.512 respectively [49, 50]. It has been difficult to distinguish two phase transitions using machine learning techniques.

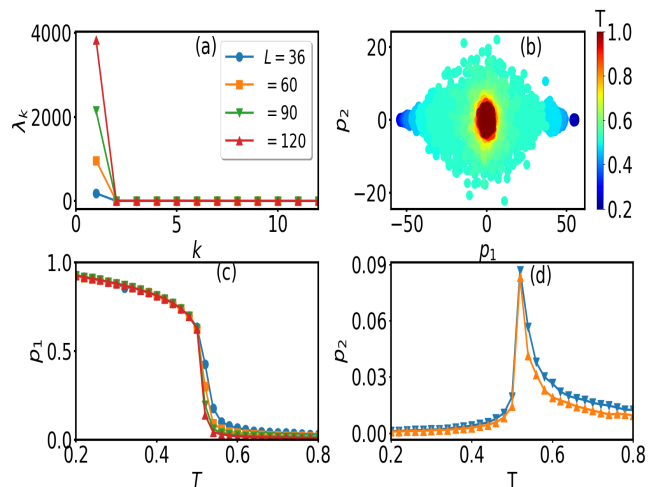


FIG. 5. PCA results of XY model on a antiferromagnetic triangular lattice by feeding the z-components of the chiral vector. We consider $M = 61$ evenly separated temperature points in the range $T = 0.2$ to $T = 0.8$ with steps $\Delta T = 0.01$. For every temperature point we consider $m = 1000$ uncorrelated data samples. (a) a dominant eigenvalue compared to others for all L (b) projection of the z-component of chiral vector along the first and second principal components, where the color-bar representing the temperature points. (c) effect of temperature on the first principal component, p_1 . p_1 suddenly decreases at the critical temperature point, $T_c = 0.512$. (d) p_2 shows peak at the phase transition temperatures.

In this work we aim to obtain both temperatures T_{BKT} and T_c accurately using PCA.

We perform PCA by feeding the z-component of the chirality Eq. 10 as input and analyze the results. We choose temperature range from 0.2 to 0.8 with steps of $\Delta T = 0.01$. At every temperature point, we generate 1000 uncorrelated samples and choose $L \times L$ system size. In the top left panel of Fig. 5(a), the first eigenvalue is much larger compared to other eigenvalues. Projecting the data into p_1 and p_2 we get the idea of the phase separation in Fig. 5(b). We note three types of regime, at high T , p_1 and p_2 are close to zero, whereas at low T , p_1 can have large values around ± 50 . In Fig. 5(c) $p_1 = \frac{1}{N_T} \sum_j p_{1j}$ is shown as a function of temperature and variation in p_1 resembles the staggered chirality as we change the temperature in the systems. A sudden decrease in p_1 at $T_c = 0.512$ indicates a phase transition and it can be associated with chirality transition. Second principal component p_2 is shown in Fig. 5(d), has a peak at the transition point T_c and resembles the specific heat. p_1 and p_2 both indicate same transition points.

Calculation of the BKT transition temperature T_{BKT} is our next goal and it is expected to be at $T_{BKT} = 0.504$. We follow the same procedure as in section III and use the vorticity as initial input to the PCA. The density of vortex ρ_v exactly matches with p_1 as shown in Fig. 6(a) for $L = 60$ and the inset shows the finite size effect

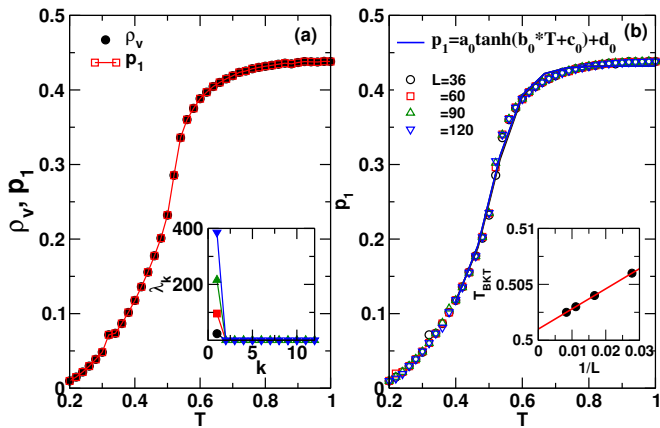


FIG. 6. PCA results for XXZ model on a 2D antiferromagnetic triangular lattice by feeding the absolute vorticity. (a) The density of vortex ρ_v , and p_1 as a function of T for different $L = 36, 60, 90$, and 120 . Eigenvalues of C_T are shown in the inset. (b) T_{BKT} is obtained by fitting p_1 with the function $a_0 \tanh(b_0 * T + c_0) + d_0$, and then equating $b_0 * T + c_0 = 0$. In the inset the finite size scaling is shown.

for L . We see an exponential increase in vortex density as well as p_1 . In Fig. 6(b) the p_1 is fitted with $p_1 = a_0 * \tanh(b_0 * T + c_0) + d_0$, where the fitting parameters in our case are $a_0 = 0.174$, $b_0 = 10.955$, $c_0 = -5.514$, and $d_0 = 0.254$ for $L = 60$ and the T_{BKT} can be evaluated by equating $b_0 * T + c_0 = 0$, i.e. $T_{BKT} = 0.5033$ which is same as the calculated value of T_{BKT} using MC technique in ref. [43]. The extrapolated value of T_{BKT} is shown in the inset of Fig. 6(b).

By analyzing the above results, one can see that even though the two transition temperatures $T_c = 0.504$ and $T_{BKT} = 0.512$ are close but our procedure can accurately calculate both the temperatures.

D. XXZ model on triangular lattice

In this subsection, the PCA is used to calculate the transition temperatures for XXZ model on a triangular lattice. The anisotropy in the z -direction Δ is tuned from 0.0 to 0.95 . In this model the $2\pi/3$ structure lies in the easy plane, besides the $SO(2)$ degeneracy the frustration causes an additional two fold degeneracy of the ground state due to chirality. The whole degeneracy belongs to $SO(2)Z_2$. The fluctuation in the out of plane direction increases with the increase of Δ and resulting in both the BKT phase transition T_{BKT} and chirality transition T_c shift to lower temperature. To calculate T_c , the z -component of the chirality vector is fed into PCA. In Fig. 7(a) we show p_1 as a function of T for $\Delta = 0.25, 0.50, 0.75$, and 0.95 . A sharp drop is seen in p_1 which resembles the staggered chirality. The eigenvalues are shown in the inset of Fig. 7(a), λ_1 is much larger compared to other eigenvalues for all L . p_2 as a function of T is shown in Fig. 7(b), we observe peaks at the critical temperatures

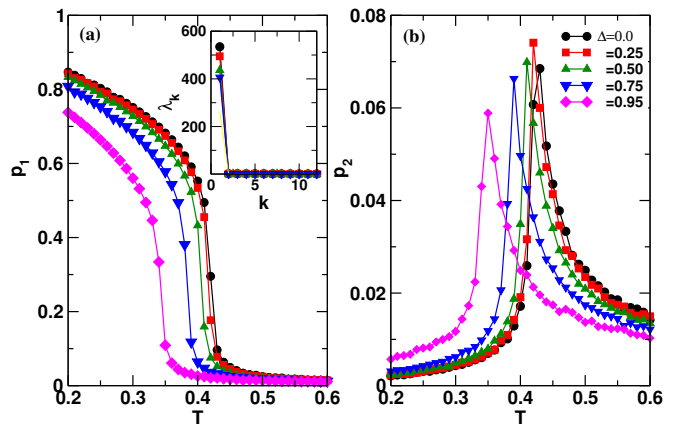


FIG. 7. PCA results of XXZ model on a 2D antiferromagnetic triangular lattice by feeding the z -component of the chiral vector for $\Delta = 0.0, 0.25, 0.50, 0.75$ and 0.95 . (a) plot of p_1 as a function of temperature for different Δ and the eigenvalues are shown in the inset. p_1 resembles staggered chirality. (b) p_2 shows a peak at the transition temperature for different Δ .

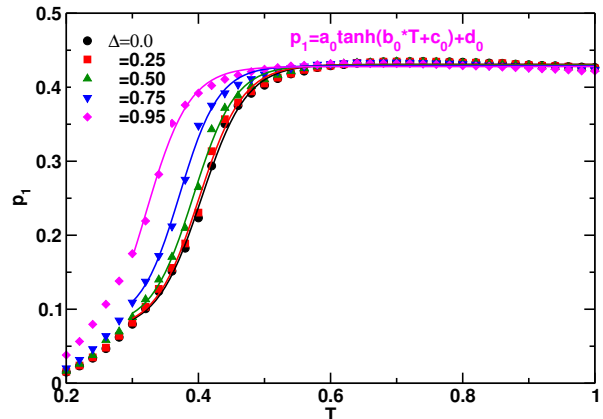


FIG. 8. p_1 as a function of temperature for XXZ model on a antiferromagnetic triangular lattice for $\Delta = 0.0, 0.25, 0.50, 0.75$, and 0.95 for a system size $L = 60$. p_1 is fitted with the function $a_0 \tanh(b_0 * T + c_0) + d_0$ to obtain the T_{BKT} .

T_c , which are consistent with reported values in ref. [43]. In Table. II our calculated T_c values are compared with reported values calculated from the MC simulation [43].

In order to estimate BKT transition temperature, absolute vorticity is fed into PCA for $\Delta = 0.0, 0.25, 0.50, 0.75$, and 0.95 and p_1 is fitted with the function $a_0 \tanh(b_0 * T + c_0) + d_0$ at the proliferation region to estimate T_{BKT} by equating $b_0 * T + c_0 = 0$ as shown in Fig. 8. The estimated values of T_{BKT} and reported values calculated by fitting in-plane correlation length ξ and in-plane susceptibility χ of the MC calculation [43] are compared in the Table. III. The extrapolated values of the T_{BKT} are also shown in the Table III.

TABLE II. Estimated long range order-disorder transition temperatures, T_c with the reported values for $\Delta = 0.0, 0.25, 0.50, 0.75,$ and 0.95 in case of XXZ model in frustrated triangular lattice. \pm values show the error of the fitting.

Δ	T_c (MC)	T_c (PCA)
0.0	0.412 ± 0.005	0.422 ± 0.002
0.25		0.420 ± 0.002
0.50	0.400 ± 0.005	0.410 ± 0.003
0.75		0.390 ± 0.004
0.95		0.350 ± 0.004

TABLE III. Estimated short-range BKT transition temperatures, T_{BKT} with the reported values calculated by fitting in-plane correlation length, ξ and in-plane susceptibility, χ for $\Delta = 0.0, 0.25, 0.50, 0.75,$ and 0.95 in case of XXZ model in frustrated triangular lattice. \pm values show the error of the fitting.

Δ	T_{BKT} (ξ fit)	T_{BKT} (χ fit)	T_{BKT} (PCA)
0.0	0.402 ± 0.002	0.403 ± 0.001	0.405 ± 0.003
0.25			0.401 ± 0.003
0.50	0.391 ± 0.002	0.388 ± 0.003	0.391 ± 0.004
0.75			0.371 ± 0.003
0.95			0.320 ± 0.004

V. SUMMARY

In this work the thermal phase transitions of the classical XXZ model on 2D lattices are studied using PCA. The ferromagnetic XY and XXZ models on the square lattice are non-frustrated, whereas, antiferromagnetic Heisenberg models are frustrated on a triangular lattice. These ferromagnetic models on the square lattice have only the BKT type transition due to the vortex-antivortex pair unbinding, whereas on the triangular lattice there are two types of thermal phase transitions; the BKT transition is due to the breaking of continuous $SO(2)$ rotational symmetry and chirality phase transition due to the breaking of discrete Z_2 reflection symmetry. In general, the separation and evaluation of the BKT and chirality transition on the triangular lattices are challenging.

The PCA could recognize the magnetic order parameter in a finite system if the spin configurations obtained

from the Monte Carlo simulation are fed as initial input to the PCA, but it fails to identify the BKT transition and chiral phase transitions in 2D systems as shown in ref [23, 26]. Alternatively the preprocessing of spin configurations is done to calculate the vorticity but the PCA analysis does not predict the T_{BKT} as the proliferation of vortex density starts much below the T_{BKT} [26]. Therefore, we fit the proliferation region with a function $a_0(1 - \frac{T_{BKT}}{T})^\alpha$ to extract T_{BKT} . As shown in Fig. 3(b) p_1 matches very well with density of vorticity and by fitting p_1 and extrapolated it gives $T_{BKT} = 0.894$ as shown inset for XY model on square lattice in Fig. 3(b). We show that calculated values from the PCA are consistent with reported value in the literature [42, 45, 46]. T_{BKT} of 2D XXZ model for different values of exchange anisotropy $\Delta = 0.0, 0.25, 0.50, 0.75,$ and 0.95 and compared with reported values in the literature and these T_{BKT} values match very well with literature as shown in the Table I.

In frustrated 2D triangular lattice both the transition temperatures T_{BKT} and T_c are very close and we use the PCA to calculate the critical temperatures. To find T_c , chirality from the raw spin configurations is calculated and the z-component of chirality vector is fed as initial input to PCA for both XY and XXZ models are shown in Fig. 5 and Fig. 7. T_{BKT} for XY and XXZ model are calculated using the absolute vorticity as initial input to the PCA and fitting the p_1 with the function $a_0 \tanh(b_0 * T + c_0) + d_0$ and these T_c and T_{BKT} are consistent with the reported values in the literature as shown in Table III.

In summary we studied the thermal phase transitions of XY and XXZ model on square and triangular lattice using the unsupervised machine learning method or the PCA method and calculated the T_{BKT} and T_c for triangular lattice and we show that the fitting of p_1 with standard function the T_c and T_{BKT} can be extracted. This approach can be used to extract critical temperature of other complex models on various geometries.

VI. ACKNOWLEDGEMENTS

M.K. thanks SERB for financial support through Grant Sanction No. CRG/2020/000754.

S.H. and S.S.R. have contributed equally to this work.

[1] Y. LeCun, Y. Bengio, and G. Hinton, *Nature* **521**, 436 (2015).
[2] Y. Guo, Y. Liu, A. Oerlemans, S. Lao, S. Wu, and M. S. Lew, *Neurocomputing* **187**, 27 (2016).
[3] A. Krizhevsky, I. Sutskever, and G. E. Hinton, *Adv. neural inf. process. syst.* **25**, 1097 (2012).
[4] E. Rosten and T. Drummond, *Computer Vision – ECCV 2006* (Springer Berlin Heidelberg, Berlin, Heidelberg, 2006) pp. 430–443.

[5] B. Zoph, V. Vasudevan, J. Shlens, and Q. V. Le, *Proc. IEEE Comput. Soc. Conf. Comput. Vis. Pattern Recognit.*, 8697 (2018).
[6] C. M. Bishop, *Machine learning* **128**, 1 (2006).
[7] M. Wu and L. Chen, *2015 Chinese Automation Congress (CAC)*, 542 (2015).
[8] J.-A. Choi and K. Lim, *ICT Express* **6**, 175 (2020).
[9] D. Liben-Nowell and J. Kleinberg, *J. American. Society. Info. Sci. Tech.* **58**, 1019–1031 (2007).

- [10] P. Galán-García, J. G. d. l. Puerta, C. L. Gómez, I. Santos, and P. G. Bringas, *Logic J. IGPL* **24**, 42 (2015).
- [11] M. R. Islam, M. A. Kabir, A. Ahmed, A. R. M. Kamal, H. Wang, and A. Ulhaq, *Health info. science and systems* **6**, 1 (2018).
- [12] I. Bose and R. K. Mahapatra, *Information & Management* **39**, 211 (2001).
- [13] A. Rajkomar, J. Dean, and I. Kohane, *New England J. Medicine* **380**, 1347 (2019).
- [14] J. VanderPlas, A. J. Connolly, Ž. Ivezić, and A. Gray, in *2012 conference on intelligent data understanding (IEEE, 2012)* pp. 47–54.
- [15] P. Baldi, K. Cranmer, T. Faucett, P. Sadowski, and D. Whiteson, *Parameterized neural networks for high-energy physics*, Vol. 76 (Springer, 2016) pp. 1–7.
- [16] V. M. Eskov, V. F. Pyatin, V. Eskov, and L. Ilyashenko, *Biophysics* **64**, 293 (2019).
- [17] M. Q. Ding, L. Chen, G. F. Cooper, J. D. Young, and X. Lu, *Mol. Cancer Res.* **16**, 269 (2018).
- [18] G. Carleo and M. Troyer, *Science* **355**, 602 (2017).
- [19] J. Carrasquilla and R. G. Melko, *Nature Physics* **13**, 431 (2017).
- [20] G. Torlai and R. G. Melko, *Phys. Rev. B* **94**, 165134 (2016).
- [21] P. Broecker, J. Carrasquilla, R. G. Melko, and S. Trebst, *Sci. rep.* **7**, 1 (2017).
- [22] L. Wang, *Phys. Rev. B* **94**, 195105 (2016).
- [23] C. Wang and H. Zhai, *Phys. Rev. B* **96**, 144432 (2017).
- [24] S. S. Schoenholz, E. D. Cubuk, D. M. Sussman, E. Kaxiras, and A. J. Liu, *Nature Physics* **12**, 469 (2016).
- [25] K. Ch’Ng, J. Carrasquilla, R. G. Melko, and E. Khatami, *Phys. Rev. X* **7**, 031038 (2017).
- [26] W. Hu, R. R. Singh, and R. T. Scalettar, *Phys. Rev. E* **95**, 062122 (2017).
- [27] K. Pearson, *The London, Edinburgh, and Dublin philosophical magazine and journal of science* **2**, 559 (1901).
- [28] I. T. Jolliffe, *Principal component analysis for special types of data* (Springer, 2002).
- [29] E. P. Van Nieuwenburg, Y.-H. Liu, and S. D. Huber, *Nature Physics* **13**, 435 (2017).
- [30] S. J. Wetzel, *Phys. Rev. E* **96**, 022140 (2017).
- [31] N. Astrakhantsev, T. Westerhout, A. Tiwari, K. Choo, A. Chen, M. H. Fischer, G. Carleo, and T. Neupert, *Phys. Rev. X* **11**, 041021 (2021).
- [32] L.-F. m. c. Arsenault, A. Lopez-Bezanilla, O. A. von Lilienfeld, and A. J. Millis, *Phys. Rev. B* **90**, 155136 (2014).
- [33] D. Bachtis, G. Aarts, and B. Lucini, *Phys. Rev. Research* **3**, 013134 (2021).
- [34] S. J. Wetzel and M. Scherzer, *Phys. Rev. B* **96**, 184410 (2017).
- [35] N. D. Mermin and H. Wagner, *Phys. Rev. Lett.* **17**, 1133 (1966).
- [36] R. Pelcovits and D. Nelson, *Phys. Lett. A* **57**, 23 (1976).
- [37] S. Hikami and T. Tsuneto, *Prog. Theor. Phys.* **63**, 387 (1980).
- [38] A. Cuccoli, V. Tognetti, and R. Vaia, *Phys. Rev. B* **52**, 10221 (1995).
- [39] V. L. Berezinskii, *Sov. Phys. JETP* **32**, 493 (1971).
- [40] J. M. Kosterlitz and D. J. Thouless, *J. Phys. C: Solid State Phys.* **6**, 1181 (1973).
- [41] J. Kosterlitz, *J. Phys. C: Solid State Phys.* **7**, 1046 (1974).
- [42] P. Olsson, *Phys. Rev. Lett.* **75**, 2758 (1995).
- [43] L. Capriotti, R. Vaia, A. Cuccoli, and V. Tognetti, *Phys. Rev. B* **58**, 273 (1998).
- [44] M. J. Beach, A. Golubeva, and R. G. Melko, *Phys. Rev. B* **97**, 045207 (2018).
- [45] S. Chung, *Phys. Rev. B* **60**, 11761 (1999).
- [46] Y. Komura and Y. Okabe, *J. Phys. Soc. Japan* **81**, 113001 (2012).
- [47] H. Kawamura and S. Miyashita, *J. Phys. Soc. Japan* **53**, 4138 (1984).
- [48] H. Kawamura and S. Miyashita, *J. Phys. Soc. Japan* **54**, 4530 (1985).
- [49] T. Obuchi and H. Kawamura, *J. Phys. Soc. Japan* **81**, 054003 (2012).
- [50] J.-P. Lv, T. M. Garoni, and Y. Deng, *Phys. Rev. B* **87**, 024108 (2013).